Coherent Structures in DNS of Turbulent Boundary Layers at Mach 3

Matthew J. Ringuette*, Minwei Wu†, and M. Pino Martín‡
Mechanical and Aerospace Engineering Department
Princeton University, Princeton, NJ

We demonstrate that the data from DNS of turbulent boundary layers at Mach 3 exhibit the same local flow features found in both supersonic and incompressible experiments, such as long, low-speed structures in the log region and hairpin vortex packets. Instantaneous plots of the streamwise mass-flux show very long low-momentum structures in the log layer. We use Taylor's hypothesis to generate a velocity map in the log region with a streamwise length of about 230δ, where δ is the boundary layer thickness. The map indicates that the low-speed structures attain streamwise lengths of order 100δ. Length scales obtained from correlations of the streamwise mass flux severely under predict the extent of these structures, most likely due to their significant meandering in the spanwise direction. A hairpin packet-finding algorithm is employed to determine the average packet properties, and we find that the streamwise length of the Mach 3 packets is less than one-third of that observed at subsonic conditions. Adopting the technique of Brown & Thomas,[1] we observe a connection between elevated levels of wall shear stress and hairpin packets. Visualization of the instantaneous turbulence structure shows that groups of hairpin packets are frequently located above the long, low-momentum structures, consistent with the very large-scale motion model of Kim & Adrian.[2]

I. Introduction

The study of coherent structures in supersonic turbulent boundary layers is important for understanding the physical mechanisms behind the turbulence generation and transport. In comparison to incompressible flows, data on the structure of supersonic flows is lacking. A review of the present knowledge can be found in Smits & Dussauge.[3] Recently, Ganapathisubramani *et al.*[4] performed wide-field digital particle image velocimetry (DPIV) in a Mach 2 turbulent boundary layer and found evidence of alternating streamwise structures of uniform low- and high-speed fluid in the log region with lengths exceeding 8δ, where δ is the boundary layer thickness. Large-scale structures have also been observed in incompressible boundary layers by Hutchins & Marusic,[5] who used a spanwise rake of 10 hotwire probes along with Taylor's hypothesis to measure structures of length greater than 20δ. Moreover, Hutchins & Marusic[5] employed a synthetic flow field to show that the spanwise meandering of such structures conceals their true length from the single-point statistics often used to determine turbulence length scales. Tomkins & Adrian,[6] Ganapathisubramani *et al.*,[7] and Hambleton *et al.*[8] performed DPIV on incompressible turbulent boundary layers in streamwise, wall-parallel planes with measurement domain lengths of about 2δ. They found evidence that the low-speed structures contained within these comparatively smaller domains are due to the induced backward flow from clusters of paired, opposite-sign vortices, consistent with the hairpin packet model proposed by Adrian *et al.*[9] These packets coupled with the low momentum structures have been found to contribute significantly to the overall Reynolds stress.[7] Kim & Adrian[2] first proposed that the larger-scale structures are due to

*AIAA Member
†AIAA Student Member
‡AIAA Member

Case	M_δ	ρ_δ (kg/m^3)	T_δ (K)	T_w/T_δ	Re_θ	$\theta(mm)$	H	$\delta(mm)$
L09	2.98	0.0907	219.55	2.58	2390	0.430	5.4	6.04
L24	2.92	0.0750	107.80	2.85	2650	0.435	5.4	8.80

Table 1. Dimensional boundary-layer-edge and wall parameters for the DNS.

Case	δ^+	L_x/δ	L_y/δ	L_z/δ	Δx^+	Δy^+	N_x	N_y	N_z
L09	325	9.1	2.3	13.8	8.0	3.0	384	256	106
L24	420	24.0	2.2	9.0	9.3	5.8	1080	160	112

Table 2. Grid resolution and domain size for the DNS.

multiple hairpin packets aligned in the streamwise direction, termed very large-scale motions (VLSM), which is supported by evidence from Hambleton *et al.*,[8] Hutchins & Marusic,[5] and Ganapathisubramani *et al.*[4] Three-dimensional visualizations of an incompressible turbulent boundary layer at low Reynolds number were presented by Delo *et al.*,[10] who observed groups of large-scale structures reaching 5δ in length that caused multiple ejections of the low-speed fluid below them. They proposed a growth mechanism for these "agglomerations," consisting of a cycle of triggered ejections followed by entrainment of the ejected fluid at the trailing edge of the cluster, which is consistent with the existence of VLSM.

Here we utilize a direct numerical simulation (DNS) database of turbulent boundary layers at a freestream Mach number of 3, with domain lengths of $L_x = 9.1\delta$ and 24δ, and demonstrate that the data exhibit the same characteristics as the previous experiments. Although DNS is a powerful tool for determining flow structure, it is critical that the simulations produce realistic physics. We investigate the occurrence of large-scale, low-speed structures in the log region, and characterize the properties of hairpin vortex packets. Additionally, we examine the connection between hairpin packets and the wall skin friction.

II. DNS parameters and accuracy

The details of the numerical method are provided in Martín.[11] The freestream conditions for the calculations are atmospheric at 20 km altitude, and the Reynolds numbers for the mean flow profiles are the maximum values for which we can gather DNS statistics in a reasonable turnaround time. The number of grid points necessary for accurate DNS is determined by the ratio of the large to small scales, $\delta^+ = \delta/z_\tau$, where z_τ is the near-wall length-scale.

Table 1 gives the boundary-layer-edge conditions for the DNS, as well as Re_θ, δ, and the relevant integral parameters. The wall condition is isothermal, and we prescribe the wall temperature to be nearly the adiabatic temperature. The grid resolution, domain size, and δ^+ for the simulations are provided in table 2. The streamwise, spanwise, and wall-normal directions are taken as x, y, and z, respectively.

Martín[11] describes the accuracy of the DNS as compared to theory and experiments. Here, we summarize these results. Figure 1 plots the van Driest transformed velocity profiles for the DNS data, showing good agreement between the prediction and the simulations. The skin friction coefficients of the DNS for $L_x = 9.1\delta$ and $L_x = 24\delta$ are 0.0021 and 0.0019, respectively, which fall within 8% of the van Driest II prediction.

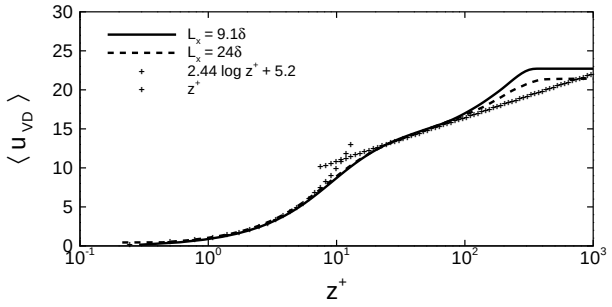

Figure 1. Mean velocity profiles for the DNS.

III. Results and comparison with experiments

A. Two-point correlations

For comparison with previous experiments, we compute two-point spatial correlations $R_{(\rho u)'(\rho u)'}$ of the streamwise fluctuating mass-flux in (x, y)-planes. The experiments considered report correlations of velocity only, but for the Mach 3 DNS the correlations of $(\rho u)'$ and u' are very similar. Figure 2(a) shows the correlation map for the 24δ domain at $z/\delta = 0.2$, within the logarithmic layer. We find elongated positive coherence in the streamwise direction, extending to 0.8δ at a contour level of 0.06, with adjacent regions of negative correlation (dashed contours). The DNS correlation map is similar to those reported by Hutchins & Marusic[5] and Ganapathisubramani *et al.*,[4] and consistent with the existence of alternating structures of low- and high-speed flow observed in both studies.

To obtain information on the size of the turbulent structures, we calculate the longitudinal and transverse integral length scales, Λ_x and Λ_y, respectively. They are computed by integrating the fluctuating mass-flux correlations for the streamwise and spanwise velocity from the origin until the value falls below 0.05, beyond which the correlation exhibits low-magnitude oscillations. At a given wall-normal location the correlation is averaged spatially for each time realization and the resulting integral scale is ensemble-averaged over multiple, independent realizations. The integral length scales as defined here represent half of the average structure length in the specified direction.

Figures 2(b) and 2(c) plot Λ_x and Λ_y, respectively, versus distance from the wall for the 24δ domain DNS. We find that Λ_x lies between about 0.3δ and 0.7δ throughout the boundary layer, consistent with the correlation map in figure 2(a). Below we demonstrate that the streamwise length scale obtained from two-point correlations significantly under predicts the true extent of the coherent structures. The plot of Λ_y shows that the structure width increases with wall-normal distance and asymptotically approaches a value of about 0.2δ at the boundary layer edge. In the log region, Λ_y, or the average structure half-width, is approximately 0.13δ, which is in agreement with the visualizations presented below.

B. Large-scale low-speed structures

Plotting contours of ρu in the log-law region of the DNS reveals large-scale, low-momentum structures similar to those found in the experiments of Hutchins & Marusic[5] and Ganapathisubramani *et al.*[4] Figure 3 gives contour plots for the $L_x = 9.1\delta$ and 24δ cases in (x, y)-planes located at $z/\delta = 0.2$; the low-speed structures are indicated by the darker contour levels. The visualizations show that these long features exhibit significant meandering in the spanwise direction. Between two and three structures fit within the 2δ width of the simulations.

To establish the importance of the low-speed structures to the overall turbulence, we compute their contribution to the total turbulence energy in (x, y)-planes at three wall-normal locations. We identify the structures by stipulating that u' should be less than a threshold. The two-dimensional u-spectra is calculated over the entire plane with the velocity at non-structure points set to zero, then integrated to obtain the energy. We consider three wall-normal locations, $z^+ = 5$ and 15, and $z/\delta = 0.2$. The thresholds at each height are $-0.05\overline{u(z)}$, $-0.10\overline{u(z)}$, and $-0.05\overline{u(z)}$, respectively. Table 3 gives the low-speed structure energy as a percentage of the total for both the 9.1δ and 24δ domains. We find that the energy content does

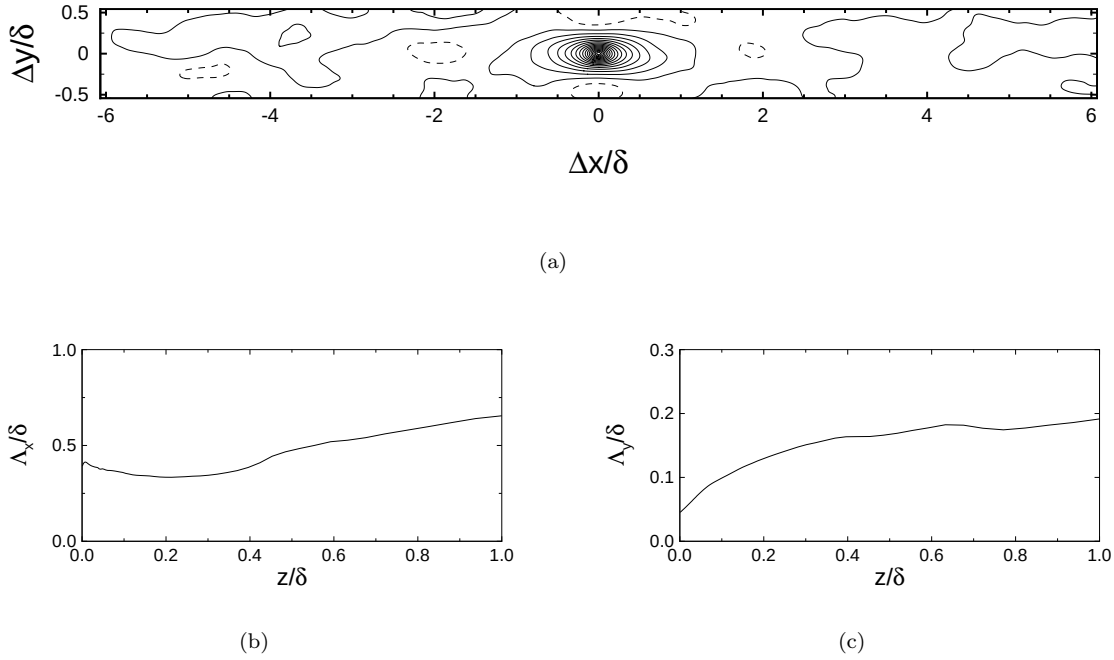

Figure 2. (a) Two-point correlation of streamwise fluctuating mass flux, $R_{(\rho u)'(\rho u)'}$, at $z/\delta = 0.2$ for $L_x = 24\delta$. Contour levels are -0.12 to 0.96 in increments of 0.06. (b) Streamwise and (c) spanwise integral length scales vs. wall-normal distance for $L_x = 24\delta$.

not change significantly with domain length. The low-speed structures contain about 24% of the streamwise turbulence energy at $z^+ = 5$, and over one-third of the energy at the buffer region and log layer locations.

Location	$L_x = 9.1\delta$	$L_x = 24\delta$
$z^+ = 5$	24.6%	23.1%
$z^+ = 15$	37.0%	35.7%
$z/\delta = 0.2$	36.8%	38.8%

Table 3. Percentage of energy contained in the low-speed structures at different wall-normal locations for domains of length 9.1δ and 24δ.

To determine an upper-limit to the streamwise length of the low-speed structures, we utilized Taylor's hypothesis of "frozen" convection to generate a long-domain velocity map. We ran this simulation for an equivalent of 300 convective time scales (δ/U_δ), and sampled the streamwise velocity at $x = 4\delta$ in intervals of one δ/U_δ apart. The data were sampled at a wall-normal location of $z/\delta = 0.2$, and a convection velocity of $0.76U_\delta$ was used to convert time into streamwise distance. Figure 4(a) gives the resulting reconstructed velocity map, which contains long regions of low streamwise velocity represented by the darkest contours. This is consistent with the instantaneous contour plots from the long-domain DNS (figure 3). These low-speed features are more evident when the higher frequency, spanwise-oriented "ripples" due to the sampling rate (at one δ/U_δ) are removed by taking the streamwise average of the velocity over $x = 0$–4δ at each time

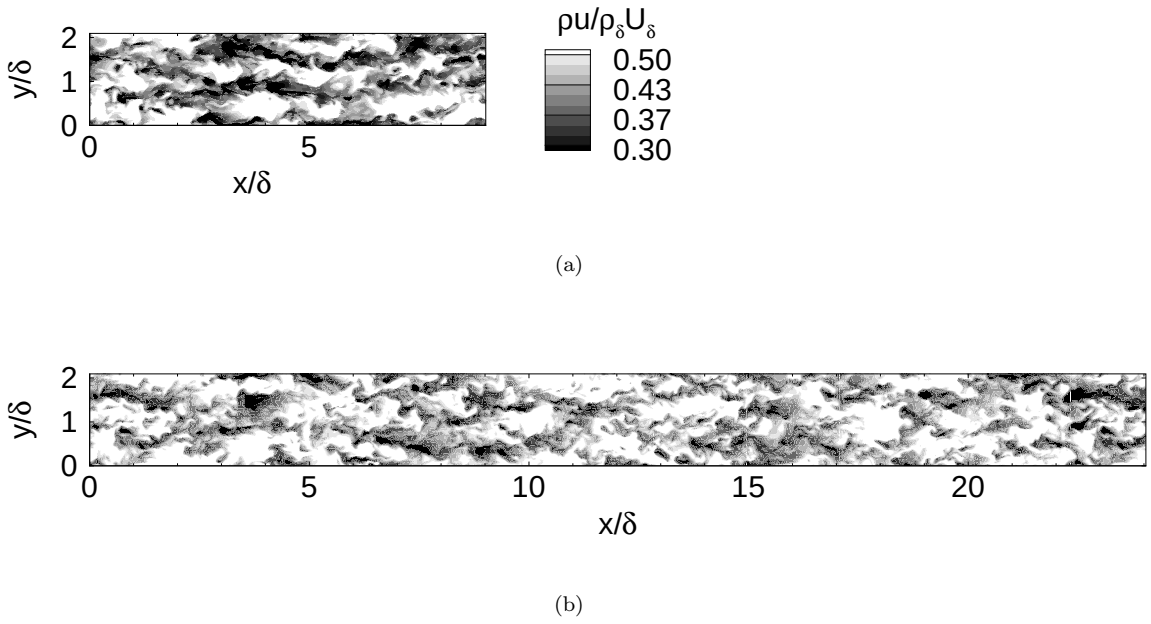

(a)

(b)

Figure 3. Contours of ρu highlighting the large-scale, low-momentum structures (given by the darker levels) in the logarithmic region for the (a) $L_x = 9.1\delta$ and (b) 24δ DNS. The planes are located at $z/\delta = 0.2$ and plotted with an x-to-y ratio of 1; the legend is the same for both data sets.

sample (figure 4(b)).

Figure 4(c) shows a similar streamwise velocity contour map from Hutchins & Marusic,[5] generated using a spanwise rake of 10 hotwire probes along with Taylor's hypothesis. The boundary layer is subsonic with $Re_\tau = 14380$. The data were taken at $z/\delta = 0.15$ and reconstructed using a convection velocity equal to the local mean; note that the effective streamwise length of the map is 20δ. Both the DNS and experimental data contain long, low-speed streamwise structures separated by regions of high velocity. One such structure extends beyond the 20δ-domain of the experiments. The DNS data show low-speed structures with length of order 100δ. We find that the width of the low-velocity features for both studies is comparable, and that their spanwise spacing is about 0.5δ. The velocity maps show that the low-speed structures of the experiments and simulations both exhibit significant spanwise meandering. This behavior was shown by Hutchins & Marusic[5] to hide the structure length from two-point statistical methods, which probably accounts for the comparatively small streamwise integral scales computed for the 9δ and 24δ DNS.

C. Hairpin packets

Inspecting the DNS data in streamwise, wall-normal planes reveals that hairpin packet "signatures," as described by Adrian *et al.*,[9] are a common phenomenon. We therefore devised a post-processing code to find packets and characterize their properties. The scheme searches (x, z)-planes for packet signatures, i.e. "head" vortices that are clustered together in the streamwise direction and form a ramp with a shallow, downstream angle relative to the wall.

We chose the swirling strength, λ_{ci}, to visualize the three-dimensional hairpin structures. The swirling strength distinguishes between vorticity coinciding with the rotating flow of compact vortices and that dominated by shear.[12] The packet-finding algorithm first identifies hairpin head vortices using the criteria that λ_{ci} must be greater than $4.5\overline{\lambda_{ci}}$ (where the over-bar indicates the mean) and that the out-of-plane vorticity is larger than 2 standard deviations from the mean; only the region between the buffer layer and the boundary layer edge is considered for both determining the threshold values and searching for hairpin packets. These criteria occasionally pick out hairpin legs, or tall vortical structures, that may or may not be attached below a hairpin head. The algorithm uses a maximum head-vortex size criterion, $0.1\delta \times 0.1\delta$, and flags identified structures that are larger than this as legs. It then checks for a head above the leg by

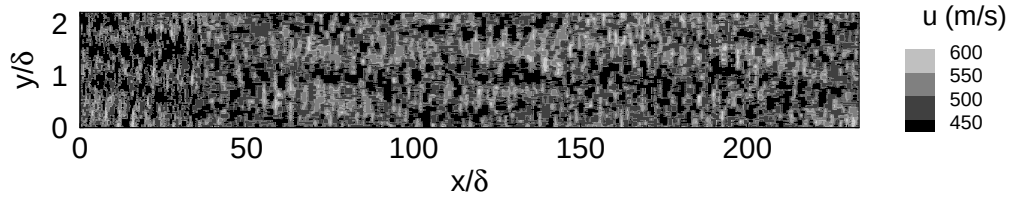

(a)

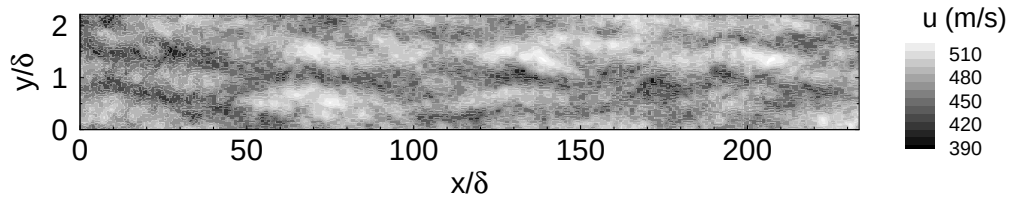

(b)

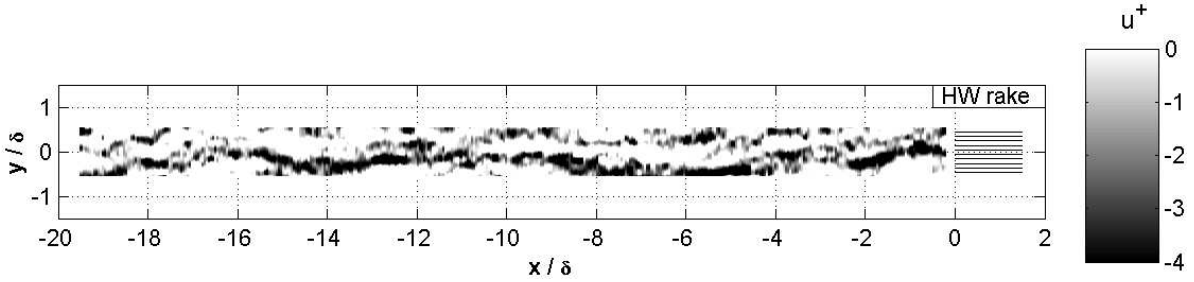

(c)

Figure 4. Example rake signal at $z/\delta = 0.2$ from DNS compared with the experimental results of Hutchins & Marusic.[5] The x-axis is reconstructed using Taylor's hypothesis; for the DNS a convection velocity based on U_δ ($\overline{U}_{0.2\delta} = 0.76U_\delta$) is used. (a) Raw data; (b) Averaged along the streamwise direction over 4δ; (c) Map of log region low-speed structures using a rake of 10 hotwire probes, adapted from Hutchins & Marusic.[5]

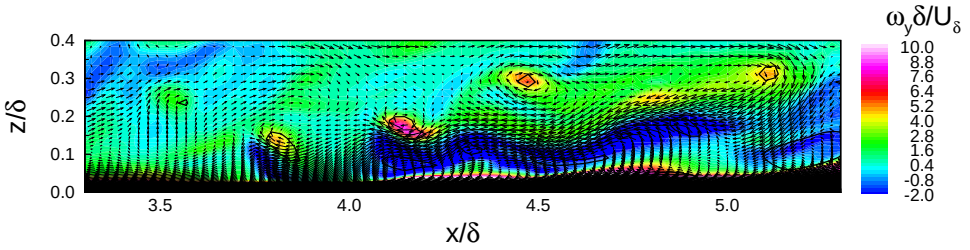

Figure 5. Streamwise/wall-normal plane through a hairpin packet in the Mach 3 DNS data, $L_x = 9.1\delta$. Contours are of spanwise vorticity, with velocity vectors and a single contour of λ_{ci}. A constant speed of $0.75U_\delta$ has been subtracted from u to highlight vortical motion.

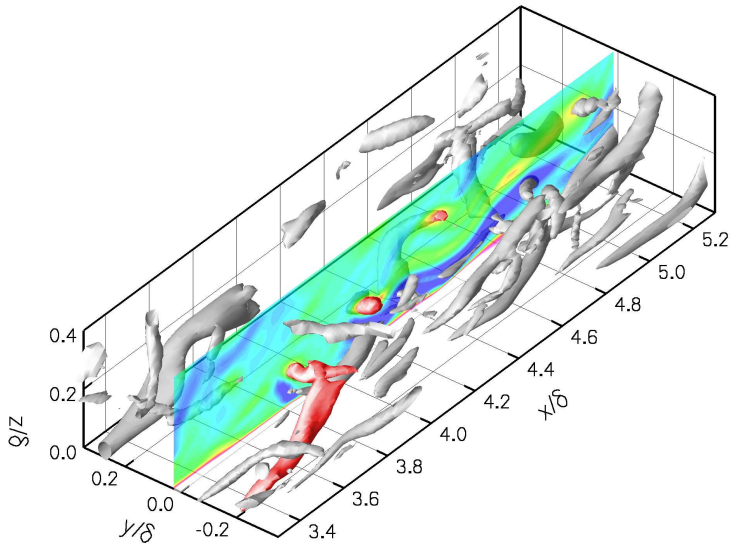

Figure 6. Hairpin vortex packet from figure 5 visualized using an iso-surface of λ_{ci}. The (x, z)-plane data of figure 5 are included for reference. The portions of the packet vortices that lie in front of this plane have been colored red.

testing whether the location of maximum λ_{ci} is within 0.1δ (the head height) from the top of the leg. If a head is found, only the head region is kept; otherwise, the structure is discarded. Next, the location of the core of each vortex is determined by assuming that it coincides with the local maximum of λ_{ci}. For each (x, z)-plane considered, the algorithm starts by choosing the vortex core that is closest to the location $(x = 0, z = z_{buffer})$ as the reference head for the first packet. It then searches for the next downstream vortex that is both within a streamwise distance of 0.5δ and at an angle of between 0° and 45° (with respect to the wall) from the reference vortex. If a vortex satisfying these criteria is found, it is considered to be part of a hairpin packet with the reference hairpin head, and is taken as the new reference vortex. The process continues until no new vortices belonging to the first packet are found. New packets are searched for in the same manner, until all identified vortices in the (x, z)-plane are accounted for. It should be mentioned that the packet-finding algorithm searches only for vortex clusters that conform to the idealized packet model.[9]

Figure 5 shows a typical packet found by the algorithm in an (x, z)-plane. Visualizing the identified structures in three-dimensions using an iso-surface of λ_{ci} verifies that the planar vortices correspond to asymmetric cane- and head-like hairpins (see figure 6).

Once any hairpin packets are identified, we determine the packet angle, α, by calculating the arctangent of the slope of the least-squares-fit through the packet vortex cores. We compute the packet convection velocity, U_{cp}, as the average streamwise velocity of the data points comprising each packet vortex. The

streamwise spacing between packets, L_p, is taken as the distance between the streamwise midpoints of each packet. Lastly, the average packet length, δ_x, height from the wall, δ_z, and streamwise head spacing, L_h, are computed from the packet vortex core positions. We generate statistics on the average packet properties by considering data in two (x, z)-planes separated by a spanwise distance of 0.75δ, so that the evaluated structures do not coincide. The results are ensemble-averaged over multiple time realizations with independent structures.

Case	δ_x (δ)	δ_z (δ)	α (°)	U_{cp}/U_∞	Heads	L_h ($^+$, δ)	L_p (δ)
AMT	1.3*	0.8(max)	12	0.6–0.8	2–10	139, 0.17†	-
GLM	$O(2)$	0.2(max)	NA	-	2–5‡	NA	-
L09	0.39	0.31	20.0	0.70	2	49, 0.15	1.33
L24	0.39	0.30	18.4	0.74	2	63, 0.15	1.36

* $Re_\theta = 7705$
† $Re_\theta = 2370$, $\delta^+ = 836$
‡ Leg pairs in (x, y)-planes

Table 4. Hairpin packet properties for streamwise domain lengths of 9.1δ and 24δ, compared with the results of Adrian *et al.*[9] (AMT) and Ganapathisubramani *et al.*[7] (GLM); see text for definitions.

Table 4 gives the average hairpin packet properties for each domain length, along with the incompressible results of Adrian *et al.*[9] at Re_θ from 930 to 7705 and Ganapathisubramani *et al.*[7] at $Re_\theta = 2500$, which is comparable to the DNS. The packet properties for the DNS do not vary significantly with domain length. We find that the streamwise length of the supersonic hairpin packets is less than one-third that of the subsonic packets at both higher and equivalent Reynolds numbers, while the number of hairpins per packet for the DNS is consistent with that reported by Ganapathisubramani *et al.*,[7] as well as Adrian *et al.*[9] at low Reynolds numbers. The average packet angle for the DNS is higher than that measured by Adrian *et al.*,[9] but within the range that they observed, and in better agreement with the value of 20° given by Head & Bandyopadhyay[13] at Re_θ of order 10000. Table 4 shows that the average hairpin spacing for the DNS is close to that of Adrian *et al.*[9] for their $Re_\theta = 2370$ case only when outer scaling is used, due to the difference in δ^+ between the experiments and the DNS. The packet convection velocity for the DNS falls within the range reported by Adrian *et al.*[9]

We investigated the effect of hairpin packets on the wall shear stress, τ_w, by correlating τ_w and u using the method of Brown & Thomas,[1] and assuming that the ramp-like structures they identified were hairpin packets. For each wall-normal location, the correlation is defined as:

$$R_{\tau_w u}(\Delta x) = \left\langle \overline{\int_{x_1}^{x_2} \tau_w'(x+\Delta x) u'(x) dx} \right\rangle / \tau_{w,RMS}' u_{RMS}'.$$

Figure 7(a) plots $R_{\tau_w u}$ at different wall-normal locations. The correlation peaks at increasing Δx as the velocity is measured farther away from the wall. Figure 7(b) plots the "enhanced" correlation. The enhanced correlation is obtained by conditionally averaging the instances in which the correlation at $z/\delta = 0.25$ is greater than 0.3 at the peak Δx location shown in figure 7(a). The result is a correlation of the same shape as shown in figure 7(a) with a much greater amplitude at different wall-normal locations. According to Brown & Thomas,[1] this is evidence for the existence of some organized structure. The angle of the structure is computed by a least square fit of the peak points at z/δ from 0.05 to 0.5 in figure 7(b), which gives a value of about 21°. This is consistent with the angle given by the hairpin packet-searching algorithm, so it is likely that hairpin packets are associated with elevated τ_w.

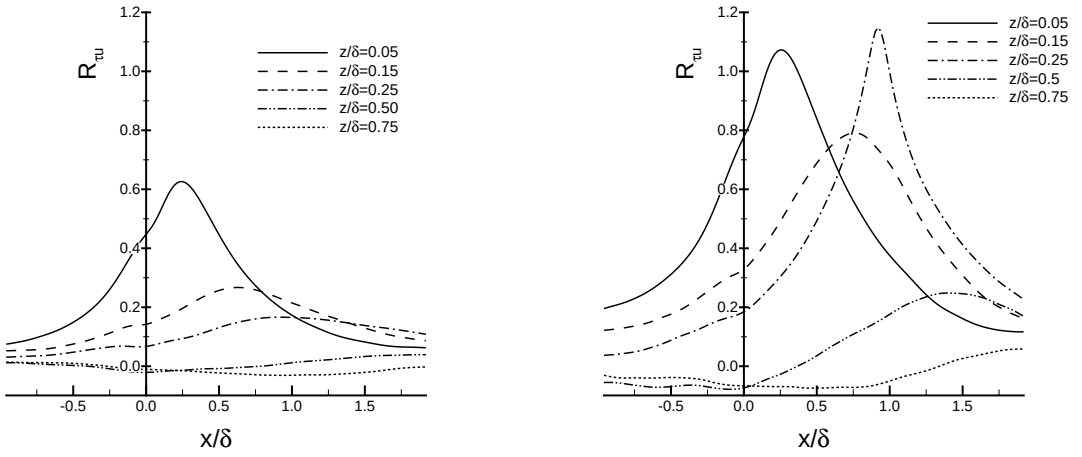

Figure 7. Time-averaged spatial correlations between wall shear stress and streamwise velocity versus streamwise distance at different wall-normal locations. (a) standard correlation; (b) "enhanced" correlation.

IV. Very large-scale motions

The small streamwise spacing (1.3δ) of the DNS hairpin packets as compared to the length of the large, low-speed structures is consistent with the VLSM model proposed by Kim & Adrian.[2] The VLSM model states that the low-speed, streamwise structures are generated by closely spaced streamwise groups of hairpin packets with significant spanwise alignment. This alignment causes the low-momentum zones below the packets to merge and form the low-speed structures. We created instantaneous visualizations to determine if the DNS data support the VLSM model.

Figure 8(a) gives an isometric view of a 9δ-long flow volume extracted from the $L_x = 24\delta$ DNS. The color contours are of streamwise velocity, with values greater than the packet convection velocity removed to highlight only the low-speed structures. This isometric view shows two perpendicular "slices," or planes, of data. The first is an (x, y)-plane located at the top of the buffer region ($z^+ = 30$), while the second is a vertical, or (x, z)-planar, slice located at $y = 0.52\delta$. Figure 8(b), which shows the volume viewed from above, i.e. facing the (x, y)-plane, indicates that much of the vertical slice at $y = 0.52\delta$ is intersected by a low-speed structure; the slice is marked in the figure by a black horizontal line. The low-speed feature does not intersect the entire vertical slice because of its spanwise meandering and streamwise termination. A second horizontal line is plotted in figure 8(b) at $y = -0.68\delta$, and represents an (x, z)-slice not shown in the isometric view of figure 8(a). This slice was chosen to provide data within a region of high-speed fluid, for comparison.

The vertical slice shown in figure 8(a) (at $y = 0.52\delta$) contains black crosses that mark the core locations of hairpin packet vortices found by the algorithm described previously. These vortices are concentrated predominantly above the zones of low-speed fluid indicated by the color contours of u. The (x, y)-planar view of figure 8(b) shows a corresponding lack of hairpin vortex heads, designated by vertical tick marks, in regions where the low-speed feature does not intersect the (x, z)-plane at $y = 0.52\delta$. There is a similar lack of hairpin packet vortices in the vertical slice above the high-speed region at $y = -0.68\delta$ (see figure 8(b)).

Figures 9(a) and 9(b) provide an instantaneous picture of the hairpin vortex structures for the same views given in figures 8(a) and 8(b), respectively, by showing an iso-surface of λ_{ci} having a value of $3.5\overline{\lambda_{ci}}$; this value is somewhat less conservative than the threshold used by the packet-finding algorithm. Consistent with the data of figure 8, figure 9 shows symmetric and asymmetric hairpin vortices clustered primarily above the regions of low-speed fluid. This lends support to the VLSM model of Kim & Adrian.[2]

V. Conclusions

We utilize a DNS database of Mach 3 turbulent boundary layers and show that the numerical data contain the same coherent structures observed in experiments at both supersonic and incompressible conditions. Contours of the instantaneous mass-flux indicate long, low-momentum structures in the DNS for both the 9δ and 24δ domain lengths. These structures exhibit significant spanwise meandering and have long streamwise lengths, consistent with previous experiments. Using Taylor's hypothesis allows for the reconstruction of a streamwise velocity map in the log region having a domain length of 230δ. The map shows meandering, low-speed structures that attain lengths of order 100δ. The spanwise meandering of these structures is the most likely reason for the discrepancy between their observed length and that obtained from the integral length scale, as this meandering would effectively mask the structures from two-point correlation methods (see Hutchins & Marusic[5]). A hairpin packet-finding algorithm is used to determine the average properties of the DNS packets. The results show that the Mach 3 packets are less than one-third the streamwise length of packets measured at incompressible conditions. We employ the enhanced correlation technique of Brown & Thomas[1] and find a connection between hairpin packets and an increase in the wall shear stress. Visualization of the instantaneous, three-dimensional turbulence structure shows streamwise groups of hairpin packets that are concentrated predominantly above the large-scale, low-speed structures. This is consistent with the VLSM model proposed by Kim & Adrian.[2] If, as the VLSM model states, the long, low-momentum features are caused by the induced backward flow from aligned "trains" of hairpin packets, then the higher levels of wall shear stress associated with packets also apply to the low-momentum structures.

Acknowledgments

We would like to acknowledge the support from the Air Force Office of Scientific Research under grant no. AF/F49620-02-1-0361 and the National Science Foundation under grant no. CTS-0238390.

References

[1]Brown, G. L. and Thomas, A. S. W., "Large structure in a turbulent boundary layer," *Phys. Fluids*, Vol. 10, No. 2, 1977, pp. 243–251.

[2]Kim, K. C. and Adrian, R. J., "Very large-scale motion in the outer layer," *Phys. Fluids*, Vol. 11, No. 2, 1999, pp. 417–422.

[3]Smits, A. J. and Dussauge, J.-P., *Turbulent shear layers in supersonic flow*, Springer, 2nd ed., 2006.

[4]Ganapathisubramani, B., Clemens, N., and Dolling, D., "Large-scale motions in a supersonic turbulent boundary layers," *J. Fluid Mech.*, Vol. 556, 2006, pp. 1–11.

[5]Hutchins, N. and Marusic, I., "Evidence of very long meandering features in the logarithmic region of turbulent boundary layers," *J. Fluid Mech.*, 2007, In press.

[6]Tomkins, C. and Adrian, R., "Spanwise structure and scale growth in turbulent boundary layers," *J. Fluid Mech.*, Vol. 490, 2003, pp. 37–74.

[7]Ganapathisubramani, B., Longmire, E. K., and Marusic, I., "Characteristics of vortex packets in turbulent boundary layers," *J. Fluid Mech.*, Vol. 478, 2003, pp. 35–46.

[8]Hambleton, W. T., Hutchins, N., and Marusic, I., "Simultaneous orthogonal-plane particle image velocimetry measurements in a turbulent boundary layer," *J. Fluid Mech.*, Vol. 560, 2006, pp. 53–64.

[9]Adrian, R., Meinhart, C., and Tomkins, C., "Vortex organization in the outer region of the turbulent boundary layer," *J. Fluid Mech.*, Vol. 422, 2000, pp. 1–54.

[10]Delo, C. J., Kelso, R. M., and Smits, A. J., "Three-dimensional structure of a low-Reynolds-number turbulent boundary layer," *J. Fluid Mech.*, Vol. 512, 2004, pp. 47–83.

[11]Martín, M. P., "DNS of hypersonic turbulent boundary layers. Part 1: initialisation and comparison with experiments," *J. Fluid Mech.*, 2007, In press.

[12]Zhou, J., Adrian, R., Balachandar, S., and Kendall, T., "Mechanisms for generating coherent packets of hairpin vortices in channel flow," *J. Fluid Mech.*, Vol. 387, 1999, pp. 353–396.

[13]Head, M. and Bandyopadhyay, P., "New aspects of turbulent boundary-layer structure," *J. Fluid Mech.*, Vol. 107, 1981, pp. 297–338.

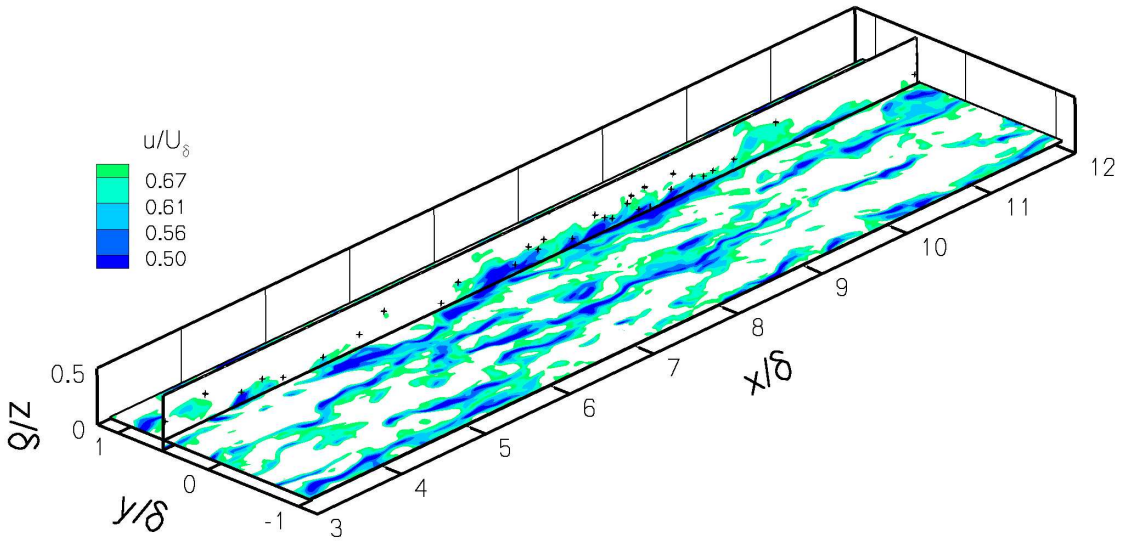

(a)

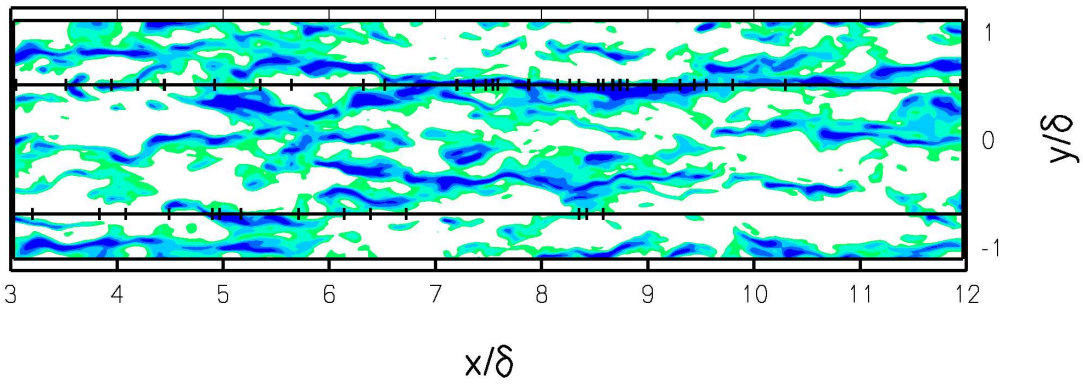

(b)

Figure 8. Visualization connecting the large-scale, low-speed regions with hairpin packets. The volumetric data shown are extracted from the $L_x = 24\delta$ DNS. Color contours are of streamwise velocity with values above the average hairpin packet convection velocity removed to highlight the large, low-speed structures. Flow is in the positive x-direction. (a) Isometric view showing an (x, z)-planar (vertical) data slice at $y = 0.52\delta$ and an (x, y)-planar (horizontal) data slice at the top of the buffer region ($z^+ = 30$). +'s indicate the location of hairpin vortex heads identified by the hairpin packet-finding algorithm as belonging to a hairpin packet. (b) (x, y)-planar (top-down) view of the same data set. Two vertical slices are marked by horizontal black lines: the slice shown in panel (a), as well as a vertical slice at $y = -0.68\delta$. The tick marks along these vertical slices denote the locations of hairpin heads found by the hairpin packet algorithm.

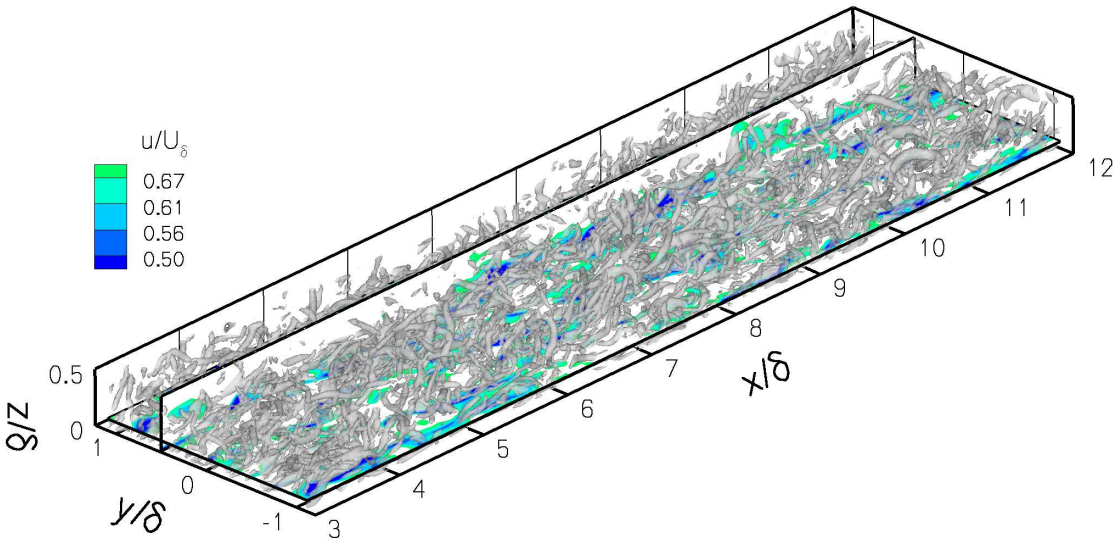

(a)

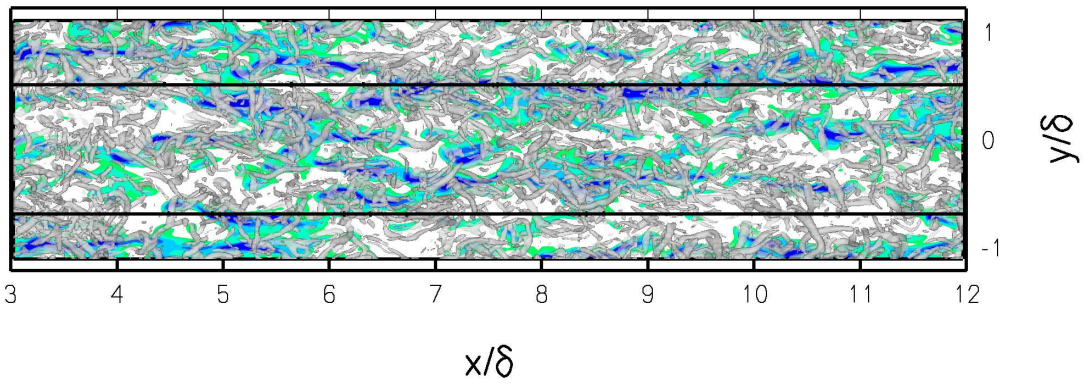

(b)

Figure 9. Visualization showing three-dimensional hairpin vortex structures in relation to the large-scale, low-speed regions. Details are the same as for figure 8, with the addition of an iso-surface of λ_{ci} at a value of $3.5\overline{\lambda_{ci}}$ used to visualize the hairpins. The iso-surface is plotted with 40% translucency so that the u-contours are visible behind it.